PERGAMON

Journal of Structural Geology 22 (2000) 1609–1620

JOURNAL OF STRUCTURAL GEOLOGY

www.elsevier.nl/locate/jstrugeo

Recognising the crystallographic signature of recrystallisation processes in deformed rocks: a study of experimentally deformed rocksalt

Patrick W. Trimby*, Martyn R. Drury, Christopher J. Spiers

Vening Meinesz Research School of Geodynamics, Faculty of Earth Sciences, Utrecht University, P.O. Box 80.021, 3508 TA Utrecht, The Netherlands

Received 3 December 1999; accepted 23 May 2000

Abstract

The microstructural development of synthetic rocksalt experimentally deformed at 100–200°C can be dominated either by grain boundary migration recrystallisation or by subgrain rotation recrystallisation, depending on water content. Samples taken from both regimes have been analysed using automated electron backscatter diffraction in order to collect crystallographic orientation and misorientation data. The frequency distribution of boundary misorientations, the boundary hierarchy characteristics and the nature of any crystallographic preferred orientation (CPO) have been used to determine the crystallographic signature of both recrystallisation processes. Dominant subgrain rotation recrystallisation results in many low to medium angle (4–20°) boundaries, a strong CPO and a continuous boundary hierarchy. Dominant grain boundary migration recrystallisation results in few low or medium angle boundaries, and a discrete boundary hierarchy. The causes of these differences and the potential application of crystallographic signatures to the study of naturally deformed rocks are discussed.

1. Introduction

The rheological and microstructural characteristics of deforming rocks are strongly influenced by dynamic recrystallisation (e.g. Sellars, 1978; Poirier and Guillopé, 1979; Avé Lallement et al., 1980; Mercier, 1980; Ranalli, 1984; Avé Lallement, 1985; Freeman and Ferguson, 1986; Rutter and Brodie, 1988). The combination of active recrystallisation mechanisms is dependent on a number of variables including pressure, temperature, strain rate, total strain, grain size and fluid content (e.g. White, 1976, 1977; Freeman and Ferguson, 1986; Handy, 1989; Hirth and Tullis, 1992; Lloyd and Freeman, 1994). Accurately identifying recrystallisation mechanisms by studying the microstructures of deformed rocks is, therefore, an essential part of the overall process of determining the deformation history.

Experimental deformation of synthetic rocksalt under conditions favouring crystal plastic flow has shown that grain boundary mobility dramatically increases when small amounts of water are present (Urai et al., 1986; Spiers et al., 1986, 1988; Spiers and Carter, 1998). In experiments carried out under confining pressures sufficient to suppress dilatancy (>10 MPa), 'wet' samples with a free water content greater than 20 ppm have boundary mobilities far greater than those found in 'dry' samples (H_2O content <10 ppm). The deformed dry samples are characterised by the formation and continued development of subgrain boundaries (polygonisation) with little or no evidence for significant grain boundary migration (Trimby et al., 2000). The wet rocksalt samples, in contrast, are characterised by extensive recrystallisation by grain boundary migration. Although subgrain boundaries do still form in the wet salt samples, the high rate of boundary migration prevents any significant development of subgrain boundary misorientation. The rapid migration rate has been linked to the observation in wet and non-dilated samples of brine films and inclusion arrays on boundary planes, and has been explained in terms of dynamic grain boundary wetting plus fluid assisted grain boundary migration (e.g. Urai, 1983, 1985; Urai et al., 1986; Spiers et al., 1988; Drury and Urai, 1990). We have used these differences in behaviour, associated with minor differences in water content, to observe microstructural development dominated by individual recrystallisation processes under controlled conditions. This provides us with an opportunity to investigate not only the microstructure resulting from a single dominant recrystallisation process, but also the crystallographic 'signature' of each process.

In this contribution, we thus compare the characteristics of microstructures dominated by subgrain rotation

* Corresponding author. Now at: HKL Technology, Blakildevej 17, DK-9500 Hobro, Denmark.

E-mail address: trimby@hkltechnology.com (P.W. Trimby).

0191-8141/00/$ - see front matter
PII: S0191-8141(00)00059-6

recrystallisation (SGRR) and grain boundary migration recrystallisation (GBMR) in the dislocation creep field, with a view to establishing criteria for recognising their operation in naturally deformed rocks. We used the electron backscatter diffraction (EBSD) technique in the scanning electron microscope (SEM) (e.g. Dingley, 1984; Wright and Adams, 1992) since conventional analysis of microstructures using light microscopy does not allow the fully quantitative measurement of crystal orientations and boundary misorientations that is necessary for a rigorous characterisation of microstructures. EBSD allows the rapid measurement of the complete crystallographic orientation of virtually any crystalline material. It has become widely used for the analysis of textures in deformed rocks (see review by Prior et al., 1999) and has been preliminarily applied to quantify misorientations in experimentally deformed rocksalt samples (Trimby et al., 2000). Using EBSD, the collection of electron backscatter patterns (EBSPs) from a grid of points on the specimen surface allows construction of a misorientation map, in which the microstructure is represented by misorientation values across individual boundaries. This allows a statistical analysis of the grain/subgrain boundary misorientation characteristics, can be used to generate boundary hierarchy data (see Trimby et al., 1998) and reveals any crystallographic preferred orientation (CPO).

2. Methodological details

2.1. Experimental set-up

The synthetic rocksalt starting material was prepared by cold pressing and annealing analytical grade NaCl (see Peach and Spiers, 1996). This produced a material with a mean grain size of 300–400 μm, although the grain sizes between individual batches varied slightly. The water content of such material was typically ≈60 ppm (measured by infrared analysis); this formed the 'wet' starting material. 'Dry' starting material was prepared by heating wet material in air for ≈24 h at 550°C. This resulted in a final water content of 2–5 ppm, but produced little or no microstructural change. Cylindrical samples of dry and wet material were axially compressed in a triaxial deformation apparatus at a confining pressure of 50 MPa. The wet sample (68 ppm water content) was deformed at 125°C at a constant displacement rate equivalent to a final strain rate of $\approx 5 \times 10^{-7}$ s^{-1}, reaching a final natural strain of 18.2%. The dry sample (<5 ppm water content) was deformed at 175°C and at a constant displacement rate equivalent to a final strain rate of $\approx 6 \times 10^{-7}$ s^{-1}, reaching a final natural strain of 53%. Note that previous experiments have shown that at strains >15% and temperatures in the range 125–175°C, microstructural development in both wet and dry material is relatively insensitive to these variables (e.g. Carter et al., 1993; Spiers and Carter, 1998). Major differences in microstructure between the samples studied will therefore be due to other factors, namely the expected recrystallisation mechanisms. Once deformation had ceased, the samples were rapidly removed from the apparatus and immediately cut into small blocks and polished following a procedure similar to that described by Spiers et al. (1986) and Urai et al. (1987). This involved mechanical grinding/polishing followed by etching in a 5% undersaturated NaCl solution for 10–30 s to remove the damaged surface layer and to render the dislocation substructure visible in reflected light. Whilst the removal of the damaged surface layer resulted in dramatically improved EBSD results over most of the sample surface studied, the increased surface relief produced reduced effectiveness near etched-out grain/subgrain boundaries. Finally, the samples were mounted and prepared for analysis in the SEM (see Trimby et al., 2000).

2.2. Microstructural analysis

Prior to SEM work, suitable areas in the wet starting material and both deformed samples were selected and imaged in reflected light using a Leica DMRX microscope. Images were captured electronically and processed using Leica's Qwin Pro v2.2 software. Although the reflected light images give a good overall impression of the microstructure, changes in etching intensity across individual boundaries only in part reflect the corresponding misorientation angle (Trimby et al., 2000). SEM analysis of selected areas was carried out using a Philips XL30 FEG SEM, typically operating with a 10 kV accelerating voltage and a system spot size 5 (beam current ≈2 nA). The relevant areas were identified by orientation contrast imaging using a forescatter detector (Prior et al., 1996).

For each area examined, EBSPs were collected from a grid of regularly spaced points either by automatically moving the electron beam, or by moving the sample and keeping the beam stationary. EBSPs were indexed using the Channel 4 software (HKL Technology) using a halite structure file consisting of 46 lattice planes. For the wet starting material and the deformed dry sample, data were collected on an orthogonal grid of 450×450 data points with a spacing of 4 μm, in order to analyse the low angle boundaries and grain-size distribution at high resolution. For the high angle boundaries and bulk texture, data points were collected from a 250×250 grid at 40 μm spacing (dry salt sample) and a 100×100 grid at 100 μm spacing (starting material). For the deformed wet sample, which has a much coarser grain size, a 350×300 grid with 25 μm spacing was used for the analysis of all boundary types. For all of the samples studied, the misorientation angle between adjacent points was calculated, taking the minimum misorientation angle out of the 24 symmetrically equivalent solutions, as is convention (e.g. Randle, 1992, 1993). Since the angular error of individual EBSD measurements is generally accepted to be <1° (Dingley and Randle,

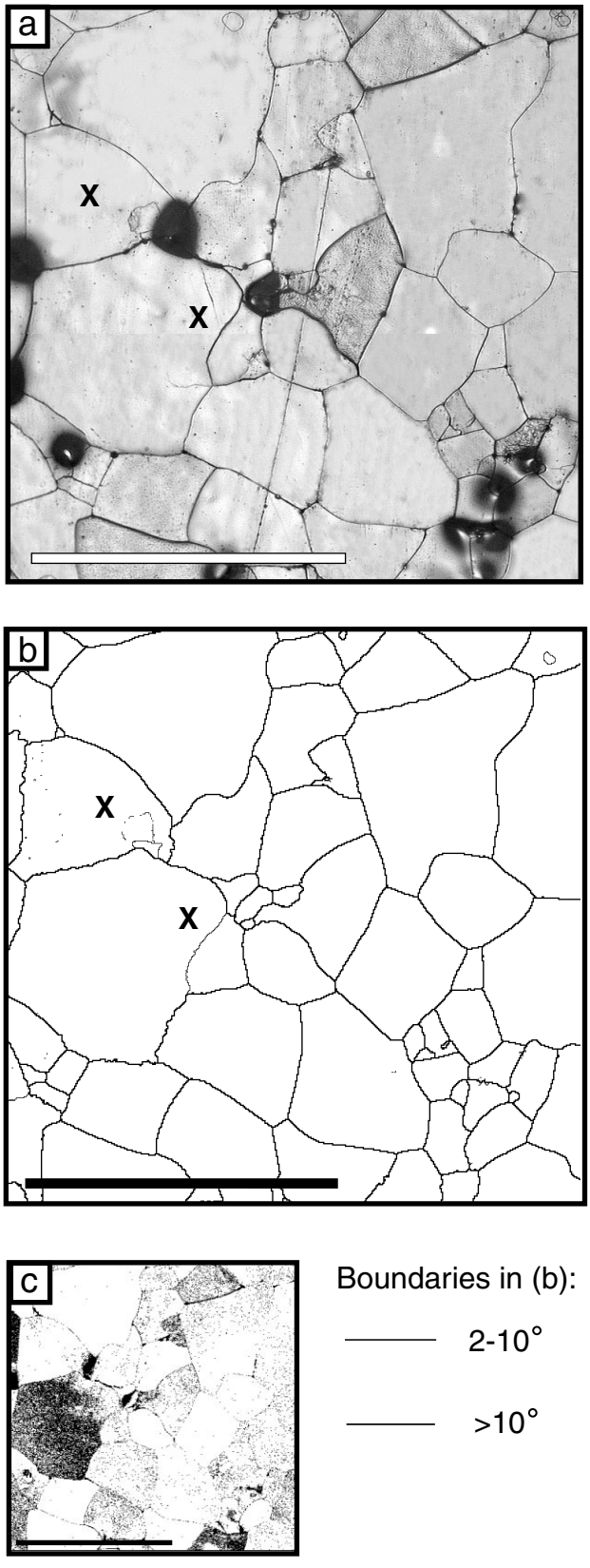

Fig. 1. Microstructure of the wet starting material. (a) Reflected light photomicrograph. Black areas are surface pits located at grain boundary fluid inclusions. (b) Misorientation map of the same area as in (a), constructed from a grid of 450 × 450 EBSD data points taken at a 4 μm spacing. (c) Map showing the EBSD indexing success rate: black dots represent data points where EBSD indexing was not possible. The scale bar in all figures represents 1000 μm. Grains containing low angle (2–10°) boundaries are marked 'X'.

1992), only boundaries with misorientations >2° can be discriminated. Using the Channel 4 software, misorientation maps for each sample were produced for boundary misorientation intervals of 2–10° and >10°. In addition, maps of the same area illustrating the position of non-indexed EBSPs were constructed. These allow assessment of the data quality, showing, for example, where surface relief, dirt particles or poor EBSP quality prevent successful pattern indexing. Inevitably minor extrapolation of orientation data for indexed points into non-indexed areas is necessary for the generation of complete misorientation maps.

Boundary misorientation frequency distributions (for both low and high angle boundaries) and grain sizes were also calculated using the misorientation maps plus Channel 4 software. To achieve this, 'grains' are defined as areas on the sample surface fully enclosed by boundaries with misorientations >10°, and grain sizes are given as equivalent circle diameters (ECDs). Since boundary misorientations have been calculated between adjacent grid points, the final boundary misorientation distributions are weighted according to individual boundary lengths: long boundaries are represented by more data than short boundaries. Rotation axes have not been considered in this study because the majority of the observed boundaries have relatively low misorientations (<15°) so that errors on individual rotation axis orientation measurements would be too great to warrant their consideration (see Prior, 1999, for a full reasoning). Note that such errors apply only to the determination of rotation axes and not to misorientation angles. The microstructural images, the misorientation maps, the boundary misorientation distributions, the grain-size data and the CPOs have been combined to help to characterise the microstructures produced by each experiment.

3. Results

3.1. Starting material

The starting material for both experiments is characterised by subpolygonal grains, ranging from 10 to 1000 μm diameter, although most fall in the range 100–500 μm, as in the wet starting material (Fig. 1a). The misorientation map (Fig. 1b) shows that only two grains in the area of analysis (marked 'X') contain subgrain boundaries with misorientations of 2–10°. The microstructure is, therefore, free from significant intragranular deformation. The quality of EBSD data is good for most of the area analysed (Fig. 2c),

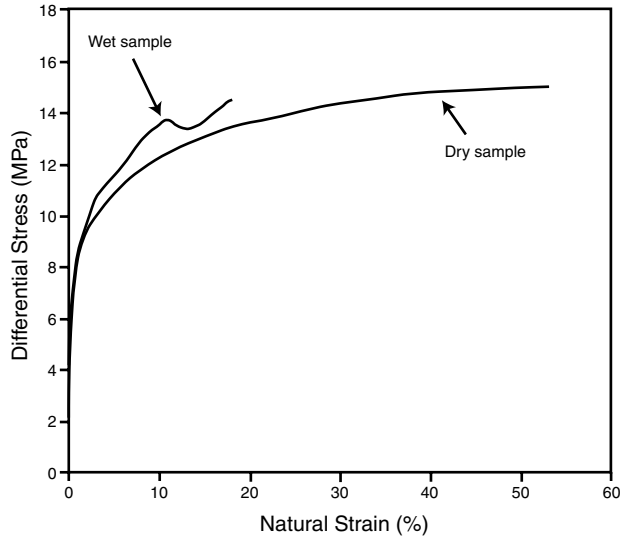

Fig. 2. Natural strain against differential stress curves for the two experiments analysed in this study. The data have been smoothed to eliminate noise.

with the exception of 2–3 grains and locations in the immediate vicinity of grain boundaries (due to high surface curvature caused by the etching procedure).

3.2. Wet salt

During deformation of the wet salt, work hardening was observed up to the final natural strain of 18.2%, with an undulation in the stress–strain curve above ≈12% strain (Fig. 2). This undulation is a characteristic feature of deformation experiments on wet synthetic salt, and usually immediately precedes mechanical steady state (Watanabe and Peach, 1999). The final microstructure was found to differ considerably from the starting material, and is dominated by the presence of large, elongate grains (long axes >4000 μm) with irregular boundaries and short axes parallel to the imposed compression direction (Fig. 3a and b). The average axial ratio of these grains is much larger than can be explained purely in terms of the applied natural strain of 18.2%. Some subgrain boundaries are optically visible within smaller grains and near grain boundaries, and larger grains show wavy slip lines in the cores (Fig. 3a). Occasional trails of inclusions appear to mark the position of ghost grain boundaries inherited from the starting material, but bear little relation to the present grain structure. The misorientation map (Fig. 3b) shows the presence of a limited number of subgrain boundaries, with misorientations of 2–10°, within many of the smaller grains, although large areas of the sample appear free from intragranular substructural features. The EBSD data were of good quality, except within one grain and in shadows cast by dirt particles on the sample surface (Fig. 3c).

Fig. 4 summarises the data on boundary misorientation and grain size in the deformed wet salt sample. The low

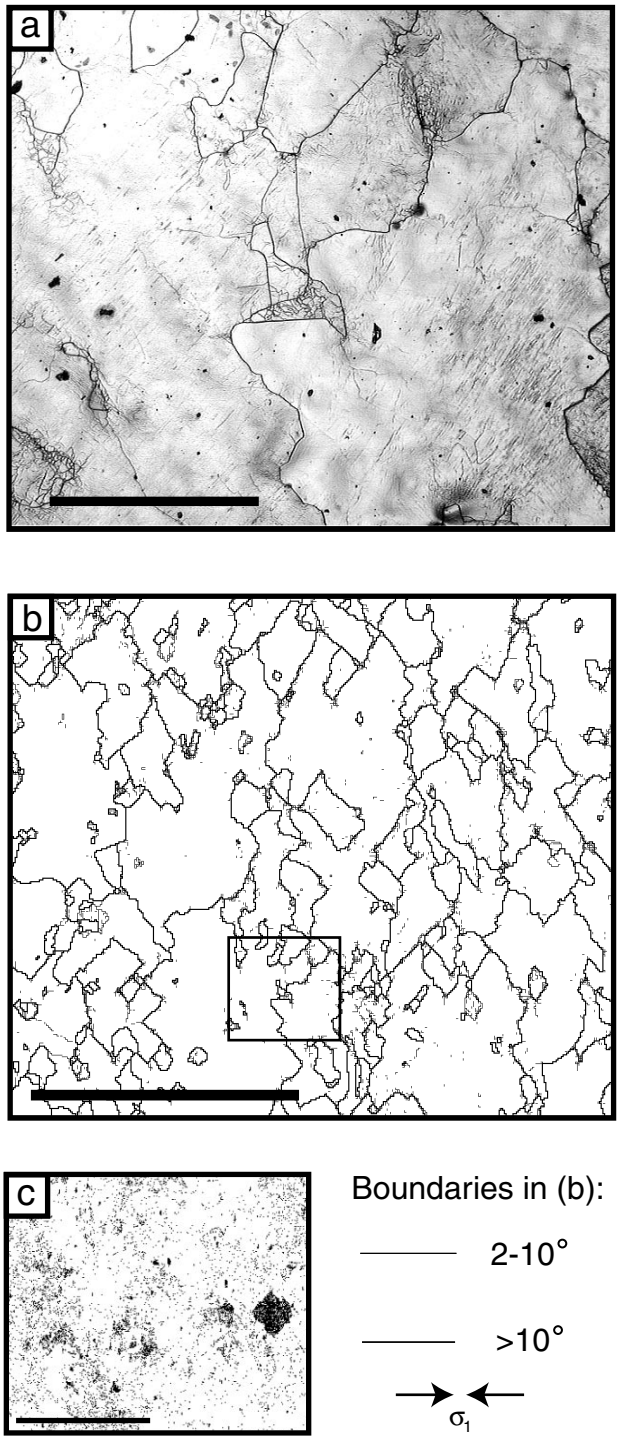

Fig. 3. Microstructure of the deformed wet salt. (a) Reflected light photomicrograph, scale bar represents 500 μm (b) Misorientation map constructed from a grid of 350 × 300 EBSD data points taken at 25 μm spacing. The black box shows the location of the area imaged in (a). (c) Map showing the EBSD index success rate: black dots represent data points where EBSD indexing was not possible. The scale bar in (b) and (c) is 4000 μm, and the compression direction (σ_1) is horizontal in all figures.

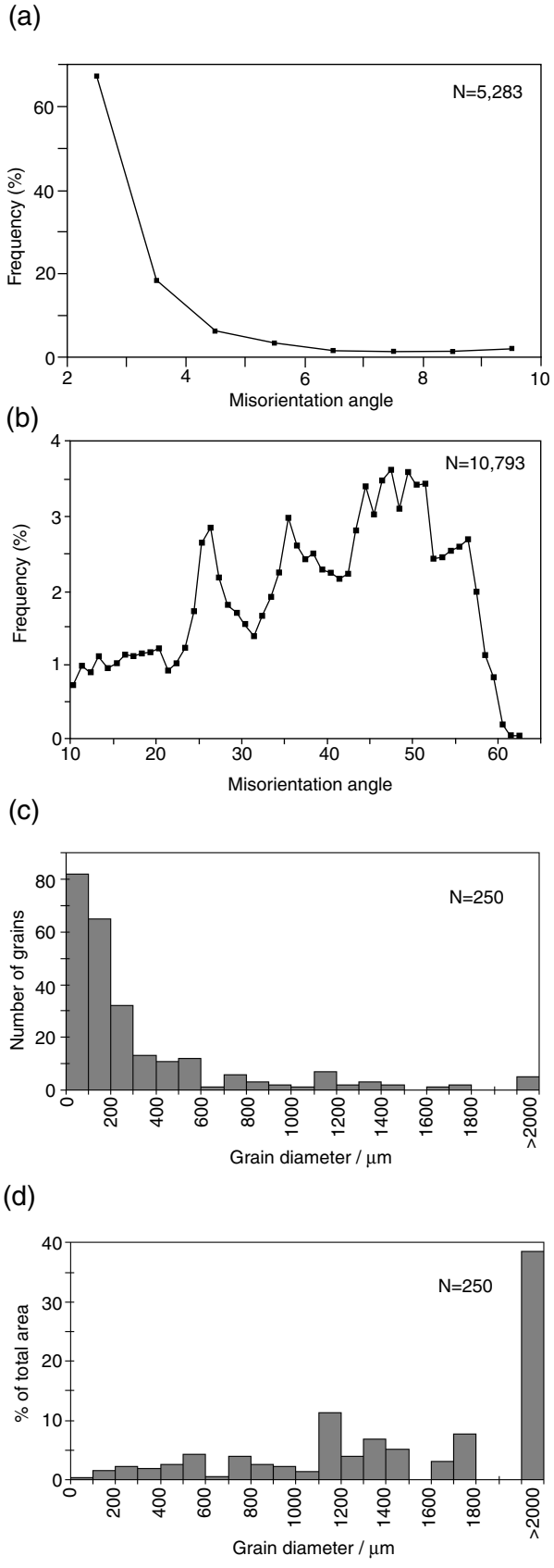

angle boundaries (Fig. 4a) are dominated by a relatively high frequency of very low angle boundaries (<3°), and a comparative absence of boundaries >4° misorientation. The high angle boundaries (Fig. 4b) show an increase in frequency up to ≈50° misorientation, and then a sudden decrease to the maximum possible misorientation of 62.8°. There is a relative lack of boundaries with misorientations in the range 4–20°. The overall distribution of boundaries >20° is not dissimilar to that expected for a population of randomly oriented cubic crystals (e.g. Mackenzie, 1964; Miodownik et al., 1999). It should be noted, however, that the present frequency distributions are generated by pixel-to-pixel measurements, and in part reflect boundary length. The long boundaries between large grains (see Fig. 3b) therefore weight the distribution shown in Fig. 4(b). The prominent peaks at misorientations of ≈26° and ≈35° can be explained by several such boundaries, and the relatively small sample size. We do not ascribe any physical significance to boundaries with these particular misorientations.

The grain-size distribution shown in Fig. 4(c) indicates an abundance of relatively small grains ($d < 300$ μm). However, in terms of the proportion of the area analysed, it is the large grains that constitute the bulk of the sample (Fig. 4d), while the small grains account for only ≈5% of the total area. It should also be noted that the small grains have diameters similar to the grains constituting the starting material (Fig. 1), although they differ in optical appearance, while the large grains are up to 1000% larger.

3.3. Dry salt

The stress–strain curve of the deformation experiment for the dry salt indicates a gradual work hardening throughout the deformation history (Fig. 2). Although steady state is approached beyond 35% natural strain (the differential stress increases only by ≈2.5% in the last 18% natural strain), the sample is still hardening. Optically the grain-size is similar to that of the starting material, but all grains show strong development of substructure and most show significant flattening (Fig. 5a). The substructure typically consists of a regular network of subgrain boundaries, and appears more strongly developed in some grains than in others. The grain boundaries generally remain straight and similar in appearance to those observed in the starting material (Fig. 1a).

The misorientation map (Fig. 5b) indicates that a significant proportion of subgrain walls have developed misorientations above 2°. Many grains contain discontinuous high angle boundaries (>10° misorientation). There is also a

Fig. 4. Boundary and grain-size distributions for the deformed wet salt sample. (a) The frequency distribution of boundaries with misorientations between 2° and 10°. (b) The frequency distribution of boundaries with misorientations >10°. (c) The grain-size frequency distribution (equivalent circle diameters). (d) The grain-size distribution expressed as the percentage contribution to the total area.

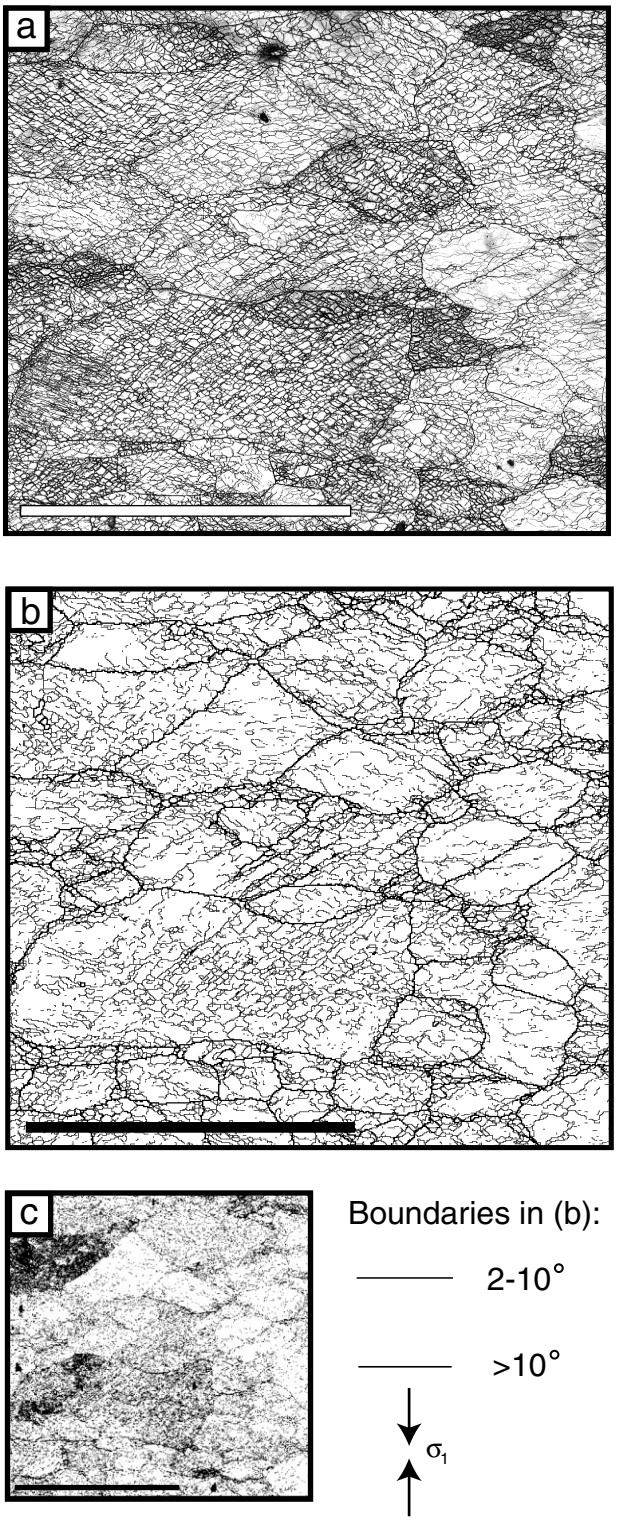

Fig. 5. Microstructure of dry salt deformed to 53% natural strain. (a) Reflected light photomicrograph. (b) Misorientation map of the same area as in (a), constructed from a grid of 450 × 450 EBSD data points taken at a 4 μm spacing. (c) Map showing the EBSD indexing success rate: black dots represent data points where EBSD indexing was not possible. The scale bar in all figures is 1000 μm, and the compression direction (σ_1) is vertical.

number of small grains ($d < 40$ μm) which are generally located at the edges of the larger grains; these are, however, infrequent. The quality of the EBSD data is variable: across most of the area the only indexing problem is that caused by boundary etching, but there are several grains where the indexing success rate was unusually low (Fig. 5c).

The boundary misorientation frequency distribution for the deformed dry material is dominated by an abundance of lower angle boundaries (Fig. 6a and b). There exist significant numbers of boundaries with misorientations between 4° and 20°, whilst the higher angle (>20°) boundary distribution approximates once again to a 'random' distribution (Fig. 6a and b). The grain size distribution for the dry sample is dominated by the abundance of very small grains ($d < 40$ μm), which make up over 50% of all the grains in the area analysed (Fig. 6c). However, these small grains constitute a minute proportion (0.66%) of the whole area of analysis (Fig. 6d).

3.4. Crystallographic preferred orientations

Pole figures showing the poles to the {100}, {110} and {111} planes for each of the three samples analysed using EBSD are shown in Fig. 7. These pole figures are derived from orientation maps of large areas of each sample (e.g. 1 cm^2), containing ≈750 grains in the starting material, 250 grains in the deformed wet sample and over 2000 grains in the deformed dry sample. In the same way that the boundary misorientation distributions are influenced by boundary length, the pole figure intensity distributions are influenced by grain size, and in the wet sample the CPO will be biased towards maxima reflecting the few very large grains.

As expected, the pole figures for the (wet) starting material have no preferred orientation (Fig. 7a). The pole figures for the deformed wet salt contain a few distinctive maxima (relating to the very large grains), with the poles to {100} noticeably aligned parallel and normal to the compression axis (σ_1) (Fig. 7b).

The pole figures for the dry sample (Fig. 7c) show evidence for a clear crystallographic preferred orientation, as well as the axial symmetry expected from axial compression. The poles to {110} are oriented parallel to σ_1, whilst the poles to {111} form a small circle at an angle of 25–30° to the σ_1 direction.

3.5. Boundary hierarchies

It was suggested by Trimby et al. (1998) that the relationship between minimum boundary misorientation angles (θ) and the size of domain that they enclose is closely related to the dominant microstructural processes. This relationship, called the boundary hierarchy, has been measured directly from the misorientation map for each sample and the results are plotted in Fig. 8. Owing to the angular errors associated with the EBSD technique, boundaries with misorientations below 2° have not been used in the hierarchy measurements.

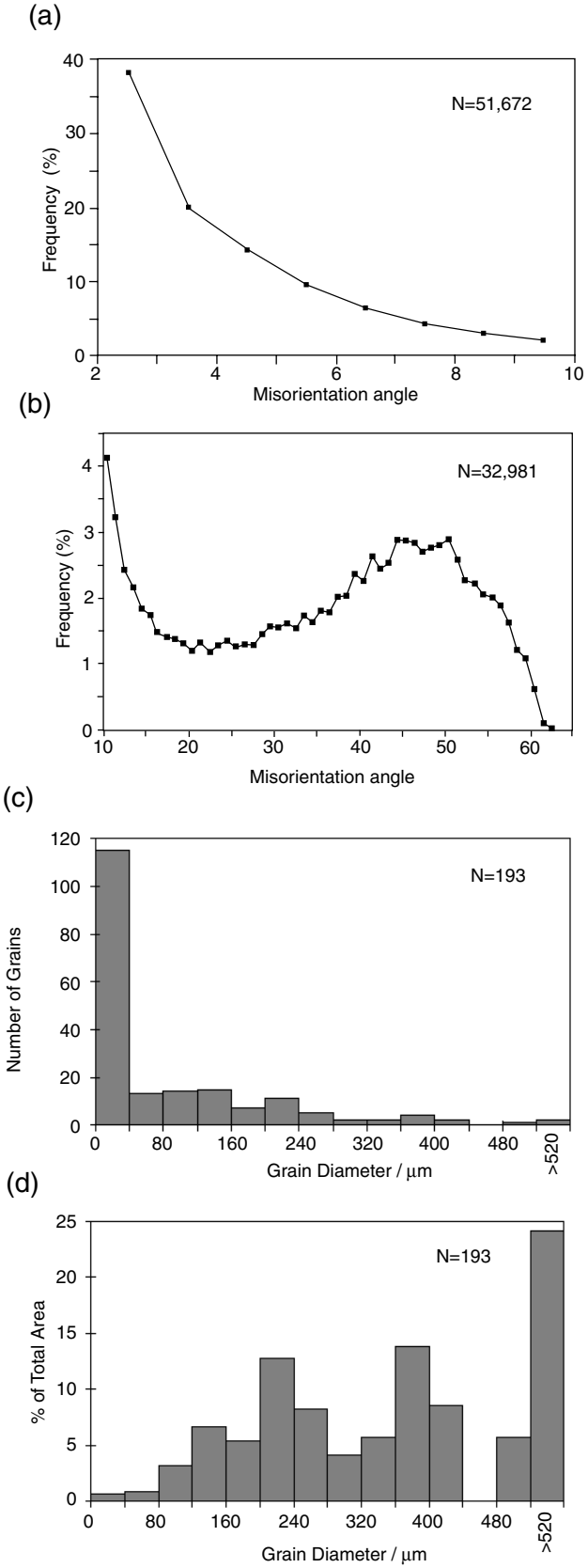

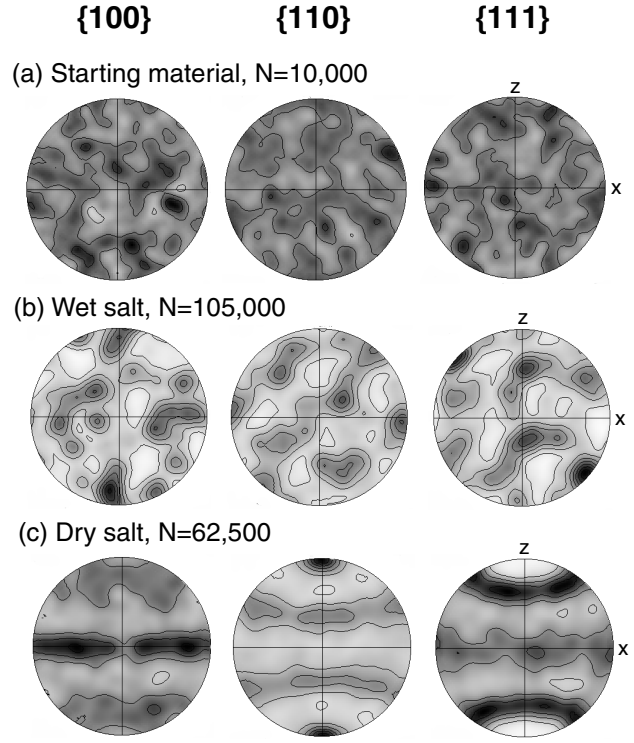

Fig. 7. Pole figures showing the CPO data for the three salt samples: for each sample the poles to {100}, {110} and {111} are shown. (a) Undeformed starting material. (b) Deformed wet salt. (c) Deformed dry salt. All pole figures are lower hemisphere, equal area plots. For the deformed samples, z represents the compression direction (σ_1). Contours are at 1, 1.5, 2, 2.5, 3 and 3.5 × random. Note that each measurement is represented by three points (for {100}), four points (for {111}) or six points (for {110}) on the pole figures. Note also that due to the sampling technique (on an orthogonal grid), the intensity distributions are influenced by grain area.

The starting material, as expected, shows no change in enclosed domain size with increasing misorientation angle. In comparison, the wet salt sample shows a much greater enclosed domain size for almost all minimum θ values, and there exists a distinct change in slope at a minimum θ of 4°: this is a 'discrete' boundary hierarchy in the terminology of Trimby et al. (1998). The dry salt sample displays a more continuous increase in domain size with increasing minimum θ value, forming a 'continuous' hierarchy. The dry sample also displays a substantial refinement of domain sizes from the starting material for all minimum θ values.

Fig. 6. Boundary and grain-size distributions for the dry salt sample deformed to 53% natural strain. (a) The frequency distribution of boundaries with misorientations between 2° and 10° (taken from the high-resolution misorientation map shown in Fig. 5b). (b) The frequency distribution of boundaries with misorientations >10° (taken from a lower resolution misorientation map of a 1 cm^2 area not shown). (c) The grain-size frequency distribution (equivalent circle diameters). (d) The grain-size distribution expressed as the percentage contribution to the total area.

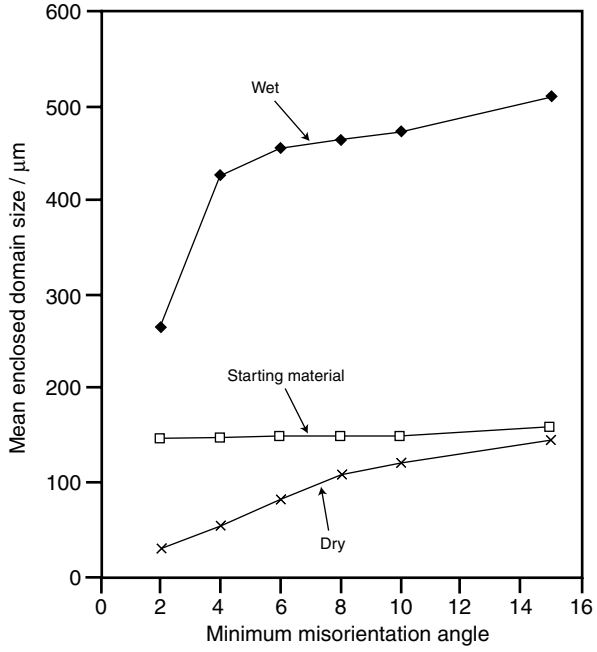

Fig. 8. Boundary hierarchy characteristics for each salt sample, showing the mean enclosed domain size plotted against the minimum misorientation angle of enclosing boundaries.

4. Discussion

4.1. Comparison between SGRR- and GBMR-dominated microstructures

The differences in appearance between SGRR- and GBMR-dominated microstructures has been recognised for a long time (e.g. Guillopé and Poirier, 1979; Urai, 1983; Lloyd and Freeman, 1994). Such discrimination is based on features such as polygonisation, neoblasts of similar size to pre-existing subgrains and core/mantle microstructures (for SGRR) vs. serrated boundaries, irregular grain shapes and variations in intragranular strain (for GBMR) (e.g. Poirier and Nicolas, 1975; White, 1976; Hobbs et al., 1976; Means, 1983; Hirth and Tullis, 1992). The deformed wet salt microstructure (Fig. 3) is dominated by a few very large, irregularly shaped grains with little internal strain (as determined from the lack of internal substructure in the misorientation map, Fig. 3b). These grains must have grown at the expense of the smaller, original grains that contained considerable internal substructure by rapid fluid-assisted grain boundary migration. The dry salt deformation microstructure (Fig. 5) is dominated by the formation of subgrain boundaries and shows no evidence for boundary migration. The observed change in grain shape is presumably due to the overall bulk deformation of the sample. Despite the occurrence of small neoblasts at the margins of some original grains, they are infrequent and the extent of recrystallisation is minimal at the strain of 53% achieved in our experiment.

Although the differences between SGRR and GBMR are readily apparent from the contrasting microstructures in the wet and dry samples, rarely will naturally deformed rocks recrystallise by one of these two processes alone, particularly at high strains. Where a balance between the two processes exists, the aforementioned expected microstructural characteristics may not be visible. Instead, the nature of the grain and subgrain boundaries (i.e. their misorientation frequency and distribution) may help to provide a more rigorous foundation upon which to base interpretations about dominant recrystallisation mechanisms, and could help the development of theoretical microphysical models. It is for this reason that it is important to compare boundary distributions corresponding to SGRR- and GBMR-dominated microstructures.

The principal difference between the distributions obtained here for wet and dry deformed samples lies in the relative abundance of ‘medium’ misorientation boundaries—i.e. boundaries with misorientations between 5° and 15°. In the deformed wet sample, there are very few boundaries with misorientations in this range (see Fig. 4), whereas the dry sample shows a high frequency of medium misorientation boundaries (Fig. 6). The relative abundance of 5–15° boundaries in the dry deformed sample is especially apparent in the higher angle misorientation frequency graph (Fig. 6b): the abundance of 10–15° misorientation boundaries dominates the frequency distribution curve. It is likely that with increased strain, more of the very low angle boundaries would develop misorientations in the range 5–15° and possibly to greater values. Although subgrain boundaries demonstrably form during deformation of the wet salt sample, sometimes developing significant misorientations (i.e. $>5°$), strongly substructured grains will be preferentially consumed by migrating boundaries, assuming that differences in internal strain and sub-boundary energy provide the driving force for migration. This process prevents a build up of medium misorientation boundaries and explains the apparent absence of 5–15° misorientations seen in some naturally deformed rocks dynamically recrystallised in a boundary migration dominated regime (e.g. Neumann, 1996; this volume). Some studies report the occurrence of medium misorientation boundaries in rocks deformed in a boundary migration regime (e.g. Trimby, 1998; Trimby et al., 1998). However, this may be related both to the presence of a strong CPO as well as to a limited component of subgrain rotation.

The boundary hierarchy characteristics for the deformed wet and dry samples are in good agreement with the predictions for GBMR- and SGRR-dominated recrystallisation given in Trimby et al. (1998). The ‘continuous’ hierarchy in the dry salt microstructure (Fig. 8) can thus be attributed to the ongoing formation of new subgrain boundaries, as well as to the progressive increase in misorientation across pre-existing subgrain boundaries. This continued formation and misorientation of subgrain boundaries as a result of ongoing recovery helps to counteract significant work

hardening. Therefore variations in internal strain energy between grains are limited (as compared to a free dislocation dominated arrangement), thus reducing the potential driving force for boundary migration. The GBMR-dominated microstructure of the deformed wet salt displays a markedly different boundary hierarchy: the increase in enclosed domain size from minimum misorientations of 2–4° (Fig. 8) can be attributed to the formation and progressive misorientation of subgrain boundaries within many of the grains. However, the rapid rate of boundary migration inhibits the formation/retention of low angle boundaries with misorientations in the range 5–15°. Hence there is little change in the enclosed domain size across this misorientation range.

The CPO of the deformed wet salt (Fig. 7b) indicates that the slip planes associated with the weakest slip system in halite at low temperatures (the $\{110\} < 1\text{–}10 >$ system) are preferentially oriented at 45° to σ_1. In accordance with Schmid's formula, this orientation would result in a maximum critical resolved shear stress on the slip planes: these grains are in a 'soft' orientation, and would deform easily. The Schmid factor on $\{110\} < 1\text{–}10 >$ has been calculated for each grain in the analysed area in the wet deformed sample, and the results are shown in Fig. 9. The large grains, with only one exception, are shaded light grey (Fig. 9a); i.e. they have Schmid factors close to 0.5, indicating that they are suitably oriented for slip on $\{110\} < 1\text{–}10 >$. In the whole of the analysed region in the deformed wet salt, 55% of the surface area has a Schmid factor >0.375 for slip on this weak system (Fig. 9b). It appears, therefore, that grains with an orientation ideal for deformation have increased in size at the expense of unfavourably oriented 'hard' grains. This is contrary to what might be expected if the soft grains developed higher dislocation densities than hard grains, since they would then be preferentially consumed via grain boundary migration. However, the deformation-based model for recrystallisation of halite proposed by Wenk et al. (1997) suggests that soft grains would, at a critical strain, recrystallise in a similar orientation by nucleation (by the onset of migration of subgrain boundaries). Extrusion experiments in halite (Skrotzki and Welch, 1983) and recrystallisation of single crystals of quartz (Hobbs, 1968) have also shown a similar nucleation and growth in the most deformed grains. It may be that the significant stress drop in the deformed wet salt experiment at 12% strain is the result of widespread nucleation (in the most deformed grains) followed by rapid growth of the newly nucleated grains (Fig. 2). However, further work is needed to clarify the development of this CPO, and its relation to the growth or consumption of particular crystal orientations.

The CPO of the deformed dry salt (Fig. 7c) can be attributed to slip on $\{110\} < 1\text{–}10 >$ (e.g. Carter and Heard, 1970; Franssen, 1993; Wenk et al., 1997). The slip system causes the {110} planes to orient perpendicular to the compression direction (σ_1) and the observed CPO (Fig. 7c) agrees with Taylor models incorporating hardening (e.g. Wenk et al., 1989; Franssen, 1993).

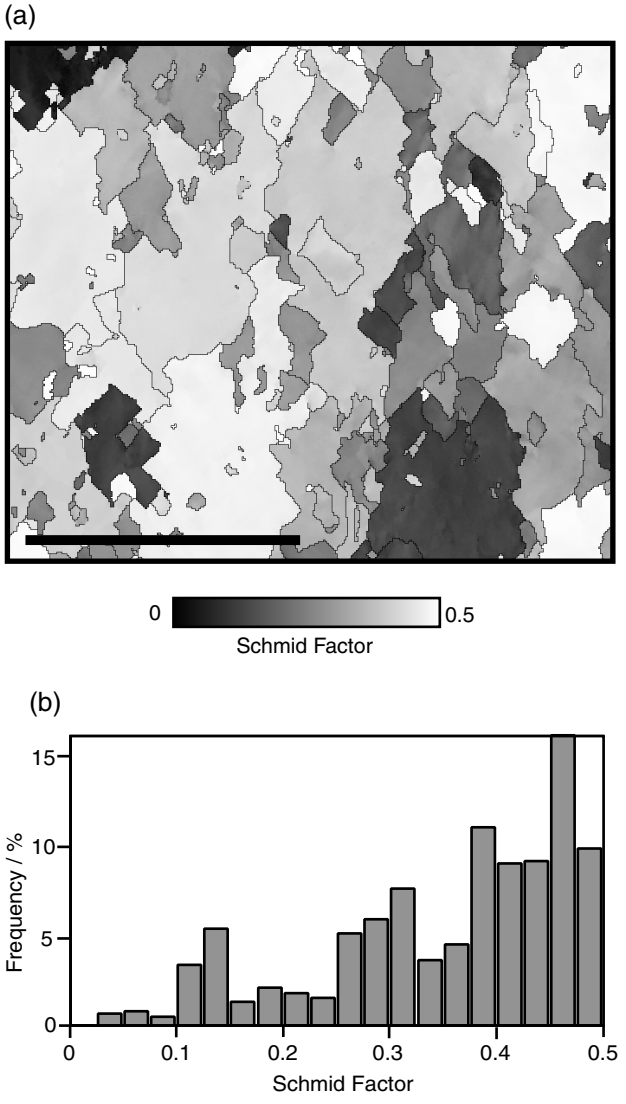

Fig. 9. (a) Misorientation map of the deformed wet salt sample, with each grid point shaded according to the maximum Schmid factor for slip on $\{110\} < 1\text{–}10 >$. Light shades indicate high factors ('soft' orientations), dark shades low factors ('hard' orientations). Scale bar is 4000 μm. (b) Histogram of frequency against Schmid factor (for $\{110\} < 1\text{–}10 >$) taken from the map shown in (a).

Whether the use of boundary misorientation distributions, CPO trends and boundary hierarchies can unequivocally identify the dominant operation of either grain boundary migration or subgrain rotation recrystallisation in a naturally deformed, completely recrystallised rock will be discussed below.

4.2. Identifying recrystallisation mechanisms in naturally deformed rocks

It is clear from the present results and from work by

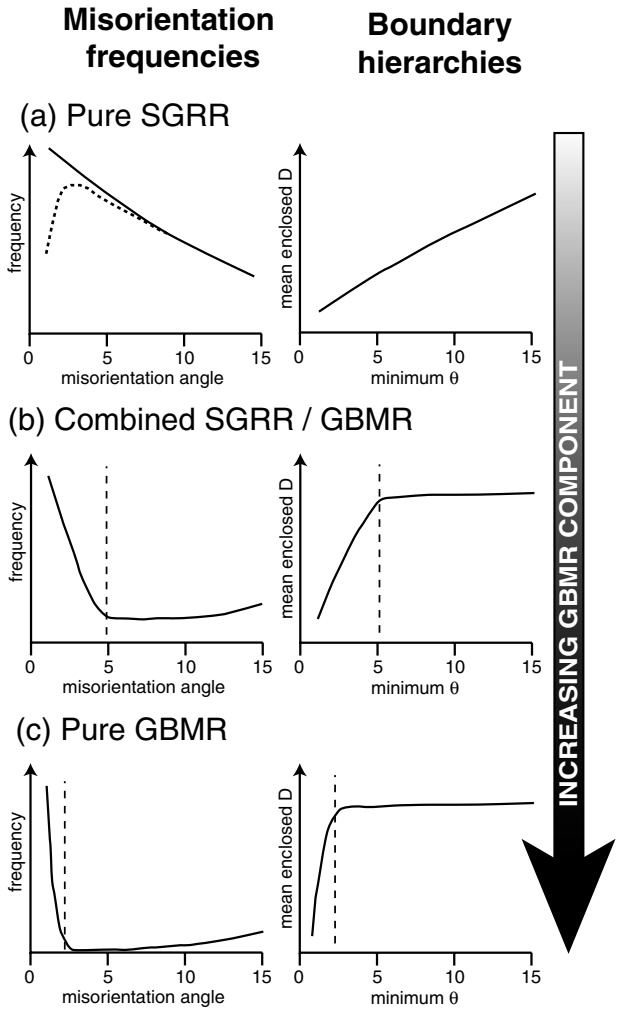

Fig. 10. Characteristic low angle boundary misorientation distributions and boundary hierarchy graphs for (a) microstructure dominated by SGRR; (b) microstructure with a component of both SGRR and GBMR; (c) microstructure dominated by GBMR. Dashed line in (a) indicates the probable misorientation distribution at higher strains, whilst dashed lines in (b) and (c) mark positions of significant changes in curve slope (see text for details).

Trimby et al. (1998) that microstructures dominated by either SGRR or GBMR are easily distinguishable. However, these are end-member scenarios and for the interpretation of naturally deformed rocks it is important to recognise the combined effects of both recrystallisation processes. The prediction and interpretation of CPO data in deformed rocks is controversial (e.g. Wenk and Christie, 1991; Bunge et al., 1994; Wenk et al., 1997), so here we shall discuss only the nature of boundary misorientation distributions and boundary hierarchies.

Fig. 10 illustrates the expected misorientation distributions for low angle boundaries and the corresponding boundary hierarchies for pure SGRR, pure GBMR and an intermediate case combining both processes. Using the present results, we are able to constrain the characteristics for both end-member scenarios with a fair degree of certainty. At higher strains we might expect a frequency peak to develop at low misorientations in the pure SGRR microstructure (dashed line in Fig. 10a), as a result of ongoing dislocation climb and glide into an already fully developed subgrain wall network. This has not yet occurred in the deformed dry salt in this study, as illustrated by the high proportion of subgrain walls which have not developed misorientations over 2° (compare Fig. 5a and b). The intermediate case, with a component of both SGRR and GBMR, will display a change in characteristics in both the misorientation frequency distribution and the boundary hierarchy. This change, marked by the dashed line in Fig. 10(b), defines the extent to which subgrain boundaries can develop misorientations before they are removed by migrating boundaries. If the change occurs at a higher misorientation angle, then the contribution of subgrain rotation to the overall microstructure development must be greater. The characteristic change in slope in both misorientation frequency distribution and in the boundary hierarchy should be recognisable in data from naturally deformed rocks, thus allowing an evaluation of the contribution of each recrystallisation process to the final microstructure.

With the increasing use of the EBSD technique, studies of low angle boundary populations in naturally deformed rocks are becoming more widespread (e.g. Trimby et al., 1998; Heidelbach et al., 2000; Neumann, this volume). Criteria, similar to those outlined in this study for GBMR and SGRR, should aid our interpretation of the recrystallisation history of microstructures in many naturally deformed rocks, and will improve our understanding of microstructure development.

5. Conclusions/summary

1. The microstructural development of experimentally deformed synthetic rocksalt is, in this study, dominated either by grain boundary migration recrystallisation (for wet salt) or by subgrain rotation recrystallisation (for dry salt).
2. The crystallographic characteristics of samples from each recrystallisation regime have been examined using EBSD and used to determine that regime's crystallographic signature.
3. Dominant subgrain rotation recrystallisation results in many low and medium angle (4–20°) boundaries, a strong CPO and a continuous boundary hierarchy.
4. Dominant grain boundary migration recrystallisation results in few low or medium angle boundaries, and a discrete boundary hierarchy.
5. Crystallographic data derived from EBSD analysis, including boundary misorientation distributions and boundary hierarchies, can be used to evaluate the relative contribution of each mechanism to the recrystallisation of naturally deformed rocks.

Acknowledgements

We would like to thank Colin Peach, Wout Pijpers and Pieter van Krieken for carrying out the deformation experiments, and Jaap Liezenberg for preparing the polished and etched samples. The electron microscopy studies were conducted at EMSA, the Utrecht University Centre for Electron Microscopy and Structure Analysis. The EBSD software was supplied by HKL Technology, Denmark. We thank Bernd Leiss, Geoff Lloyd and an anonymous reviewer for their constructive criticisms that helped to improve this manuscript. PWT and MRD gratefully acknowledge funding from an NWO-PIONIER subsidy. The wet rocksalt sample was deformed in the framework of a project on salt rheology (CJS) funded by Shell (Houston).

References

Avé Lallement, H.G., 1985. Subgrain rotation and dynamic recrystallization of olivine, upper mantle diapirism, and extension of the Basin-and-Range province. Tectonophysics 119, 89–117.

Avé Lallement, H.G., Mercier, J.-C.C., Carter, N.L., Ross, J.V., 1980. Rheology of the upper mantle: inferences from peridotite xenoliths. Tectonophysics 70, 85–113.

Bunge, H.J., Siegesmund, S., Skrotzki, W., Weber, K., 1994. In: Bunge, H.J., Siegesmund, S., Skrotzki, W., Weber, K. (Eds.). Textures of Geological Materials, DGM Informationgesellschaft mbH, Germany.

Carter, N.L., Heard, H.C., 1970. Temperature and rate dependent deformation of halite. American Journal of Science 26, 193–249.

Carter, N.L., Horseman, S.T., Russell, J.E., Handin, J., 1993. Rheology of rocksalt. Journal of Structural Geology 15, 1257–1271.

Dingley, D.J., 1984. Diffraction from sub-micron areas using electron backscattering in a scanning electron microscope. Scanning Electron Microscopy 1984-II, 569–575.

Dingley, D.J., Randle, V., 1992. Microstructure determination by electron back-scatter diffraction. Journal of Materials Science 27, 4545–4566.

Drury, M.R., Urai, J.L., 1990. Deformation-related recrystallization processes. Tectonophysics 172, 235–253.

Franssen, R.C.M.W., 1993. Rheology of synthetic rocksalt. Geologica Ultraiectina 113, 221p.

Freeman, B., Ferguson, C.C., 1986. Deformation mechanism maps and micromechanics of rocks with distributed grain sizes. Journal of Geophysical Research 91, 3849–3860.

Guillopé, M., Poirier, J.P., 1979. Dynamic recrystallization during creep of single-crystalline halite: an experimental study. Journal of Geophysical Research 84, 5557–5567.

Handy, M.R., 1989. Deformation regimes and the rheological evolution of fault zones in the lithosphere: the effects of pressure, temperature, grainsize and time. Tectonophysics 163, 119–152.

Heidelbach, F., Kunze, K., Wenk, H.-R., 2000. Texture analysis of a recrystallized quartzite using electron diffraction in the scanning electron microscope. Journal of Structural Geology 22, 91–104.

Hirth, G., Tullis, J., 1992. Dislocation creep regimes in quartz aggregates. Journal of Structural Geology 14, 145–159.

Hobbs, B.E., 1968. Recrystallization of single crystals of quartz. Tectonophysics 6, 353–401.

Hobbs, B.E., Means, W.D., Williams, P.F., 1976. An Outline of Structural Geology. John Wiley & Sons, New York.

Lloyd, G.E., Freeman, B., 1994. Dynamic recrystallisation of quartz under greenschist conditions. Journal of Structural Geology 16, 867–881.

Mackenzie, J.K., 1964. The distribution of rotation axes in a random aggregate of cubic crystals. Acta Metallurgica 12, 223–225.

Means, W.D., 1983. Microstructure and micromotion in recrystallization flow of octachloropropane: a first look. Geologische Rundschau 72, 511–528.

Mercier, J.-C.C., 1980. Magnitude of the continental lithospheric stresses from rheomorphic petrology. Journal of Geophysical Research 85, 6293–6303.

Miodownik, M., Godfrey, A.W., Holm, E.A., Hughes, D.A., 1999. On boundary misorientation distribution functions and how to incorporate them into three-dimensional models of microstructural evolution. Acta Materialia 47, 2661–2668.

Neumann, B., 1996. Texturbildende Prozesse in rekristallisierten Quarzpolykristallen—Einzelkorn—und Gesamttexturanalysen. Geotektonische Forschungen 87, 154.

Neumann, B., 2000. Texture development of recrystallised quartz polycrystals unravelled by orientation and misorientation characteristics. Journal of Structural Geology 22, 1695–1711.

Peach, C.J., Spiers, C.J., 1996. Influence of plastic deformation on dilatancy and permeability development in synthetic salt rock. Tectonophysics 256, 101–128.

Poirier, J.-P., Guillopé, M., 1979. Deformation induced recrystallization of minerals. Bulletin of Mineralogy 102, 67–74.

Poirier, J.-P., Nicolas, A., 1975. Deformation induced recrystallisation due to progressive misorientation of subgrains, with special reference to mantle peridotites. Journal of Geology 83, 707–720.

Prior, D.J., 1999. Problems in determining the misorientation axes, for small angular misorientations, using electron backscatter diffraction in the SEM. Journal of Microscopy 195, 217–225.

Prior, D.J., Trimby, P.W., Weber, U.D., Dingley, D.J., 1996. Orientation contrast imaging of microstructures in rocks using forescatter detectors in the scanning electron microscope. Mineralogical Magazine 60, 859–869.

Prior, D.J., Boyle, A.P., Brenker, F., Cheadle, M.C., Day, A., Lopez, G., Peruzzo, L., Potts, G.J., Reddy, S., Speiss, R., Timms, N.E., Trimby, P.W., Wheeler, J., Zetterström, L., 1999. The application of electron backscatter diffraction and orientation contrast imaging in the SEM to textural problems in rocks. American Mineralogist 84, 1741–1759.

Ranalli, G., 1984. Grain size distribution and flow stress in tectonites. Journal of Structural Geology 6, 443–447.

Randle, V., 1992. Microtexture Determination and its Applications. The Institute of Materials, London.

Randle, V., 1993. The measurement of grain boundary geometry. Electron Microscopy in Materials Science Series. Institute of Physics Publishing, Bristol.

Rutter, E.H., Brodie, K., 1988. The role of tectonic grain size reduction in the rheological stratification of the lithosphere. Geologische Rundschau 77 (I), 295–308.

Sellars, C.M., 1978. Recrystallization of metals during hot-deformation. Philosophical Transactions of the Royal Society London A-288, 147–158.

Skrotzki, W., Welch, P., 1983. Development of texture and microstructure in extruded ionic polycrystalline aggregates. Tectonophysics 99, 47–62.

Spiers, C.J., Carter, N.L., 1998. Microphysics of rocksalt flow in nature. In: Aubertin, M., Hardy Jr, H.R. (Eds.). The Mechanical Behavior of Salt IV—Proceedings of the Fourth Conference. Series on Rock and Soil Mechanics, Trans Tech Publications, pp. 115–128.

Spiers, C.J., Urai, J.L., Lister, G.S., Boland, J.N., Zwart, H.J., 1986. The influence of fluid–rock interaction on the rheology of salt rock, European Communities Commission, Nuclear Science and Technology Series, EUR10399.

Spiers, C.J., Urai, J.L., Lister, G.S., 1988. The effect of brine (inherent or added) on rheology and deformation mechanisms in salt rock. In: Hardy Jr, H.R., Langer, M. (Eds.). The Mechanical Behaviour of Salt: Proceedings of the Second Conference. Series on Rock and Soil Mechanics, Trans Tech Publications, pp. 89–102.

Trimby, P.W., 1998. Quantifying microstructures—the development and application of a new technique to quartzitic shear zones. Unpublished Ph.D. thesis, University of Liverpool, 125 pp.

Trimby, P.W., Prior, D.J., Wheeler, J., 1998. Grain boundary hierarchy development in a quartz mylonite. Journal of Structural Geology 20, 917–935.

Trimby, P.W., Drury, M.R., Spiers, C.J., 2000. Misorientations across etched boundaries in deformed rocksalt: a study using electron backscatter diffraction. Journal of Structural Geology 22, 81–89.

Urai, J.L., 1983. Water assisted dynamic recrystallization and weakening in polycrystalline bischofite. Tectonophysics 96, 125–127.

Urai, J.L., 1985. Water-enhanced dynamic recrystallization and solution transfer in experimentally deformed carnallite. Tectonophysics 120, 285–317.

Urai, J.L., Means, W.D., Lister, G.S., 1986. Dynamic recrystallization of minerals. In: Hobbs, B.E., Heard, H.C. (Eds.). Mineral and Rock Deformation: Laboratory Studies—The Paterson Volume, American Geophysical Union Geophysical Monograph, 36, pp. 161–199.

Urai, J.L., Spiers, C.J., Peach, C.J., Franssen, R.C.M.W., Liezenberg, J.L., 1987. Deformation mechanisms operating in naturally deformed halite rocks as deduced from microstructural investigations. Geologie en Mijnbouw 66, 165–176.

Watanabe, T., Peach, C.J., 1999. Tracking of fluid assisted grain boundary migration during plastic deformation of halite rocks via electrical impedance measurements. EOS Transactions, American Geophysical Union Fall Meeting 1999 80 (46), F964.

Wenk, H.-R., Christie, J.M., 1991. Comments on the interpretation of deformation textures in rocks. Journal of Structural Geology 13, 1091–1110.

Wenk, H.-R., Canova, G.R., Molinari, A., Mecking, H., 1989. Texture development in halite: comparison of Taylor model and self-consistent theory. Acta Metallurgica 37, 2017–2029.

Wenk, H.-R., Canova, G.R., Bréchet, Y., Flandin, L., 1997. A deformation-based model for recrystallization of anisotropic materials. Acta Materialia 45, 3283–3296.

White, S.H., 1976. The effects of strain on the microstructures, fabrics and deformation mechanisms in quartz. Philosophical Transactions of the Royal Society of London A283, 69–86.

White, S.H., 1977. Geological significance of recovery and recrystallisation processes in quartz. Tectonophysics 39, 143–170.

Wright, S.I., Adams, B.L.A., 1992. Automatic analysis of electron backscatter diffraction patterns. Metallurgical Transactions 23A, 759–767.